Solid-State Electronics 63 (2011) 49–54

Contents lists available at ScienceDirect

Solid-State Electronics

journal homepage: www.elsevier.com/locate/sse

Modeling of current–voltage characteristics of thin film solar cells

M.A. Mannan, M.S. Anjan, M.Z. Kabir *

Department of Electrical and Computer Engineering, Concordia University, 1455 de Maisonneuve West, Montreal, Quebec, Canada H3G 1M8

ARTICLE INFO

Article history:
Received 23 November 2010
Received in revised form 5 May 2011
Accepted 18 May 2011
Available online 15 June 2011

The review of this paper was arranged by Prof. S. Cristoloveanu

Keywords:
Thin film solar cells
Modeling
Carrier trapping
Charge collection
Cadmium telluride
CIGS
Amorphous silicon

ABSTRACT

An analytical model is developed to study the current–voltage characteristics of thin film solar cells by incorporating exponential photon absorption, carrier trapping and carrier drift in the absorber layer. An analytical expression for the external voltage dependent photocurrent is derived by solving the continuity equation for both electrons and holes assuming the electric field remains uniform in the absorber layer. The analytical results are verified with the numerical self-consistent solution of the steady-state continuity equations and the Poisson's equation. The overall load current is calculated considering the actual solar spectrum. It is found that the solar cell efficiency critically depends on the transport properties of the carriers that drift towards the bottom contact. The recombination current dominates over the ideal diode current in CdTe based solar cells. The theoretical model is fitted with the published experimental data on various thin film solar cells and shows a very good agreement.

1. Introduction

The second-generation thin film solar cells are increasingly promising for their cheaper production and better efficiency. Cells based on (i) polycrystalline CdTe, (ii) polycrystalline $CuIn_{1-x}Ga_xSe_2$ (CIGS) and (iii) hydrogenated amorphous Si (a-Si:H) absorbers are the three most potential photoconductors for thin film solar cells because of their excellent efficiency [1]. The subscript x represents the mole fraction. The CdTe based solar cells have a superstrate device structure of glass/SnO_2/CdS/CdTe/metal and the CIGS based solar cells have a substrate device structure of grid/ZnO/CdS/CIGS/Mo/glass [2,3] as shown in Fig. 1. Both the CdTe and CIGS based cells are p–n heterojunction cells, where a very thin layer (~0.1 μm) of CdS acts as a highly doped n-layer and CdTe or CIGS layer acts as lightly doped p-type absorber layer. The thickness of the p-layer is few micrometers. The incident photons are mainly absorbed in the p-layer and the photocarriers are collected by the built-in electric field in this layer. The a-Si:H solar cells use p-i-n type structure where the p and n-layers are few nm and the i-layer is ~1 μm thick. The incident photons are mainly absorbed in the i-layer in a-Si:H solar cells. The voltage dependent charge collection in the depleted absorber layer is the dominant charge collection mechanisms in thin film solar cells [3,4].

There has been an active theoretical and experimental research to improve the performance of these devices. Hegedus et al. reviewed a few theoretical models to describe the current–voltage (J–V) characteristics in thin film solar cells [5]. They have shown that the most successful model calculates the photocurrent by considering carrier drift and utilizing Hecht collection efficiency formula in the nearly intrinsic absorber layer [5]. However, the previous model has made an unrealistic assumption that all the carriers are generated at the top interface of the absorber layer for all incident photons. The previous model has also used a number of fitting parameters such as maximum photocurrent with complete charge collection, reverse saturation current, effective attenuation coefficient, series resistance and carrier ranges. In this paper, we solve the continuity equation for both electrons and holes considering exponential photon absorption, exponential electron–hole pair generation across the absorber layer, carrier trapping and carrier drift in the absorber layer. We obtain an analytical expression for the external voltage V dependent photocurrent assuming the electric field remains uniform in the absorber layer. The analytical results are verified with the numerical self-consistent solution of the steady-state continuity equations and the Poisson's equation. The overall load current is calculated considering the effect of voltage dependent forward dark current and the actual solar spectrum.

The present model only uses carrier ranges and series resistance as fitting parameters and thus eliminates other fitting parameters such as reverse saturation current and effective attenuation

* Corresponding author. Fax: +1 514 848 2802.
E-mail address: kabir@encs.concordia.ca (M.Z. Kabir).

0038-1101/$ - see front matter © 2011 Elsevier Ltd. All rights reserved.
doi:10.1016/j.sse.2011.05.010

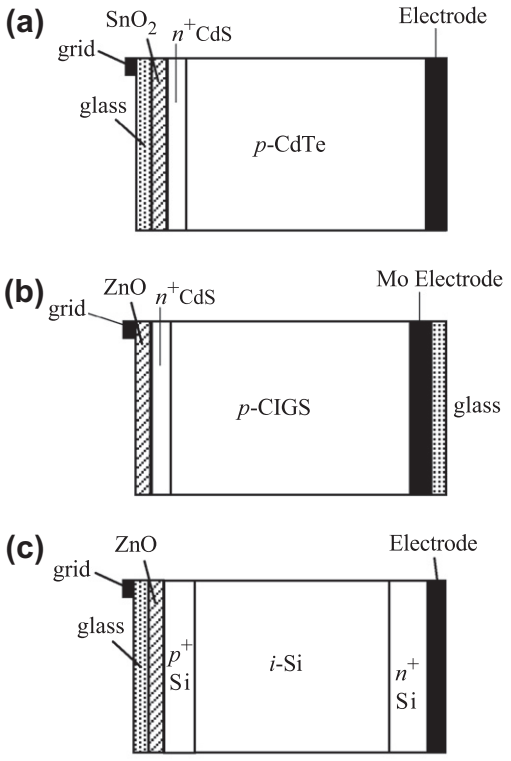

Fig. 1. Schematic diagrams representing the structures of (a) CdTe/CdS, (b) CIGS, and (c) a-Si:H solar cells.

coefficient. We analyze the J–V characteristics and efficiency in CdTe solar cells with varying carrier transport properties and operating conditions. The model is verified with the published experimental data on all three types of solar cells mentioned above. The fitting of the model with the published experimental data considering the actual solar spectrum determines the carrier transport properties (mobility-lifetimes), and the amount of reflection and scattering losses in various solar cells.

2. The model

The net external current density from a solar cell is

$$J(V) = J_d(V) - J_L(V), \tag{1}$$

where $J_d(V)$ and $J_L(V)$ are the forward diode current and photocurrent densities respectively. The forward diode current density can be written as,

$$J_d(V) = J_0 \exp\left[\frac{e(V - JR_s)}{AkT}\right], \tag{2}$$

where e is the elementary charge, R_s is the effective series resistance including all contact resistances, J_0 is the reverse saturation current of the p–n or p-i-n junction, A is the diode ideality factor, k is the Boltzman constant, and T is the absolute temperature. Since the depletion region is thick, recombination current within the depletion region should be dominant over ideal diffusion current [2]. Assuming a constant electric field in the depletion region, the reverse saturation current density can be written as [6,7],

$$J_0 = \frac{en_iW}{\sqrt{\tau'_e\tau'_h}}, \tag{3}$$

where n_i is the intrinsic carrier concentration of the absorber layer W is the width of the light absorber layer (e.g., the p-layer in CdTe or CIGS and i-layer in a-Si:H solar cells), and τ' is the carrier lifetime. The subscripts e and h refer to electrons and holes respectively.

The photon absorption in the highly doped top p or n layers will contribute a negligible current because of their very short diffusion length and very thin width. The electron–hole pair generation rate in the absorber layer can be written as,

$$G(\lambda) = \alpha(\lambda)e^{-\alpha_1 d}[1 - R(\lambda)]\lambda I_0(\lambda)/hc, \tag{4}$$

where $\alpha(\lambda)$ is the absorption coefficient of the absorber layer, λ is the photon wavelength, c is the speed of light, h is the Plank constant, I_0 is the intensity of the solar spectra (W/cm^2 nm), R is the total reflection and scattering loss factor, α_1 and d are the absorption coefficient and thickness of the thin top semiconductor layer (the n-layer in CdTe or GIGS, and p-layer in a-Si:H solar cells). The other losses include shading from the grid, absorption in the top SnO_2 layer, and incomplete electron–hole pair (EHP) generation in the absorber layer [3].

The photogenerated electrons and holes are drifted in opposite directions by the built-in electric field in the absorber layer (CdTe, GIGS or intrinsic a-Si:H layer). Electrons drift towards the radiation-receiving contact (top contact) and holes drift towards the bottom contact in CdTe or CIGS solar cells. Unlike CdTe solar cells, holes drift towards the radiation receiving contact (top contact) and electrons drift towards the bottom contact in a-Si:H solar cells.

The electric field profile in the depleted absorber layer depends on its background doping or impurity concentration. The electric field is practically uniform in low-doped absorber layer and thus the layer becomes completely depleted. On the other hand, the electric field profile becomes triangular for the uniformly distributed space charges at high level doping (this may occur in CdTe or CIGS solar cells) and thus the absorber layer may not be completely depleted as shown in Fig. 2. An analytical expression for the photocurrent can be obtained under uniform electric field whereas a numerical model is necessary to model the photocurrent under non-uniform electric field. Therefore, the models for calculating the photocurrent are described for the two cases; (1) low-doped and (2) high-doped absorber layer.

2.1. Photocurrent at low-doped absorber layer

The following assumptions are made to allow the problem to be analytically tractable: (i) The thermal equilibrium concentration of charge carriers is negligibly small because of high bandgap materials, (ii) the absorber layer is fully depleted and the built-in electric field F is nearly uniform across the absorber layer because of its lightly doping, (iii) the diffusion of carriers is negligible compared with their drift in the fully depleted absorber region, (iv) a constant

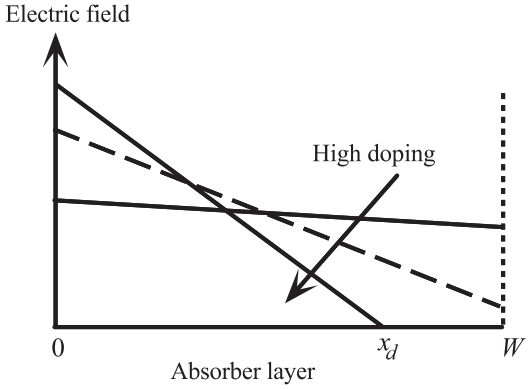

Fig. 2. Electric field dropping across the absorber layer of CdTe or CIGS solar cells with charged background impurities.

drift mobility μ and a single lifetime τ' are assigned to each type of carriers (holes and electrons). The voltage dependent electric field near the top interface of the absorber layer is slightly higher than that near the bottom interface, the photogenerated carriers will drift with a slightly higher velocity near the top interface compared to that near the bottom interface. Therefore, assuming an average drift velocity of the carriers throughout the absorber layer will not make any significant difference in the calculation of charge collection.

Considering the assumptions mentioned above, the steady-state continuity equation for the carriers that drift towards the bottom electrode is,

$$\frac{\partial c_b}{\partial t} = -\mu_b F \frac{\partial c_b}{\partial x} - \frac{c_b}{\tau'_b} + Ge^{-\alpha x} = 0, \tag{5}$$

where x is the depth in the absorber layer from the top interface of this layer, G is the carrier generation rate at $x = 0$, c_b is the photogenerated carrier concentration of the charge carriers drifting towards the bottom contact, and the subscript b refers to the carrier type drifting towards the bottom contact. For example, the subscript b represents holes (h) in CdTe solar cells. Since the carriers start drifting immediately after generation, $c_b\ (x = 0) = 0$. Therefore, the solution of Eq. (1) is,

$$c_b(x,\lambda) = \frac{G\tau'_b}{1-\alpha\mu_b F\tau'_b}\left(e^{-\alpha x} - e^{\frac{-x}{\mu_b F\tau_b}}\right). \tag{6}$$

The photocurrent density for the carriers drifting towards the bottom contact is [8,9],

$$\begin{aligned} j_b(\lambda,V) &= \frac{e\mu_b F}{W}\int_0^W c_b(x,\lambda)dx \\ &= \frac{eGW}{\left(\tau_b^{-1}-\Delta^{-1}\right)}\left[\Delta\left(1-e^{-\frac{1}{\Delta}}\right) - \tau_b\left(1-e^{-\frac{1}{\tau_b}}\right)\right], \end{aligned} \tag{7}$$

where Δ ($=1/\alpha W$) is the normalized absorption depth, τ_b ($=\mu_b\tau'_b F/W$) is the normalized carrier lifetime (carrier lifetime per unit transit time) for the carriers drifting towards the bottom contact. Since F is voltage dependent, τ_b is also voltage dependent and so does j_b.

Similarly, the photocurrent density for the carriers drifting towards the top contact is,

$$j_t(\lambda,V) = \frac{eGW}{\left(\tau_t^{-1}+\Delta^{-1}\right)}\left[\Delta\left(1-e^{-\frac{1}{\Delta}}\right) - \tau_t\left(e^{\frac{-1}{\Delta}} - e^{-\frac{1}{\Delta}-\frac{1}{\tau_t}}\right)\right], \tag{8}$$

where $\tau_t = \mu t\tau'_t F/W$ and the subscript t refers to the carrier type drifting towards the top contact (e.g., the subscript t represents electrons in CdTe solar cells). The resultant photocurrent density, $j_L(\lambda,V) = j_b(\lambda,V) + j_t(\lambda,V)$. Therefore, the photocurrent density,

$$\begin{aligned} j_L(\lambda,V) = eGW\Big\{&\left(\tau_b^{-1}-\Delta^{-1}\right)^{-1}\left[\Delta\left(1-e^{\frac{-1}{\Delta}}\right) - \tau_b\left(1-e^{-\frac{1}{\tau_b}}\right)\right] \\ &+ \left(\tau_t^{-1}+\Delta^{-1}\right)^{-1}\left[\Delta\left(1-e^{\frac{-1}{\Delta}}\right) - \tau_t\left(e^{-\frac{1}{\Delta}} - e^{-\frac{1}{\Delta}-\frac{1}{\tau_t}}\right)\right]\Big\} \end{aligned} \tag{9}$$

The total photogenerated current density is obtained by integrating over all incident photon wavelengths of the solar spectrum, i.e.,

$$J_L(V) = \int_0^\infty j_L(\lambda,V)d\lambda. \tag{10}$$

The external voltage dependent electric field is given by [3],

$$F(V) = \frac{V_0 - V_j}{W} = \frac{V_0 - (V - JR_s)}{W}, \tag{11}$$

where V_j ($=V - JR_s$) is the junction voltage, and V_0 is the flat-band voltage so that $J_L(V) = 0$ at $(V - JR) = V_0$. The flat-band voltage V_0 is slightly higher (typically ~0.1 V) than the open circuit voltage V_{OC}. It is expected that the electric field reduces to zero when the applied junction voltage is equal to the built-in potential V_{bi}. However, it is found that the electric field collapses to zero just beyond V_{OC} and slightly less than V_{bi} [3,5]. Therefore, V_0 is considered as a fitting parameter.

2.2. Photocurrent at high-doped absorber layer

Solving Poisson's equation the voltage dependent electric field distribution can be written as,

$$F(x,V) = \frac{V_0 - (V - JR_s)}{x_d} - \frac{eN_a}{\varepsilon}(x - x_d/2), \tag{12}$$

$$\text{where } x_d = \sqrt{\frac{2\varepsilon[V_0 - (V - JR_s)]}{eN_a}} \text{ and } x_d \leqslant L. \tag{13}$$

Here x_d is the width of the depletion region, N_a and ε are the doping concentration and the permittivity of the absorber layer respectively.

The steady-state continuity equation for the carriers that drift towards the bottom electrode is,

$$-\mu_b\frac{\partial(FC_b)}{\partial_x} - \frac{c_b}{\tau'_b} + Ge^{-\alpha x} = 0. \tag{14}$$

Eqs. (12) and (14) are simultaneously solved in MATLAB to find $c_b(x)$. The photocurrent density for the carriers drifting towards the bottom contact is,

$$J_b(\lambda,V) = \frac{e\mu_b}{x_d}\int_0^{x_d} F(x,\lambda,V)c_b(x,\lambda,V)dx. \tag{15}$$

Similarly, the photocurrent density for the carriers drifting towards the top contact, $j_t(\lambda,V)$, can be calculated. The resultant photocurrent density, $j_L(\lambda,V) = j_b(\lambda,V) + j_t(\lambda,V)$. The total photogenerated current density, $J_L(V)$, can be obtained by using Eq. (10).

3. Results and discussions

The J–V characteristics of various solar cells are calculated by iteratively solving above equations. The incident photon flux $I_0(\lambda)$ is taken as the air mass (AM) 1.5 global spectrum from the ASTM G-173-03 standard [10]. The theoretical model is applied to all three different thin film solar cells mentioned above.

3.1. CdTe solar cells

The theoretical model is verified by fitting with the published experimental data on CdTe solar cells. The doping concentration is CdTe layer is $\sim 10^{14}\,cm^{-3}$ [11]. The absorption coefficients for CdTe and CdS are obtained from the absorption curves in Ref. [11]. Fig. 3 shows the J–V curves of a CdS/CdTe solar cell at three sun intensities (100%, 32%, and 10% of 1.5 AM global spectrum). The CdTe layer was deposited by vapor transport (VT) method. The symbols represent experimental data, the dashed lines represent the simulation results using the numerical model, and the solid lines represent the theoretical fit to the experimental data using the analytical model. The experimental data were extracted from Fig. 6 of Ref. [6]. The CdTe thickness is 3.5 μm and the doping concentration is assumed as $10^{14}\,cm^{-3}$. The CdS thickness is assumed as 0.1 μm. The analytical model shows a very good agreement with the experimental data. The analytical and the numerical models show almost identical results (the numerical model predicts slightly less current than the numerical model). The voltage dependent electric field near the top interface of the absorber layer can be higher than that near the bottom interface, the photogenerated carriers will drift with a higher velocity near the top interface compared to that near the bottom interface. Therefore, assuming

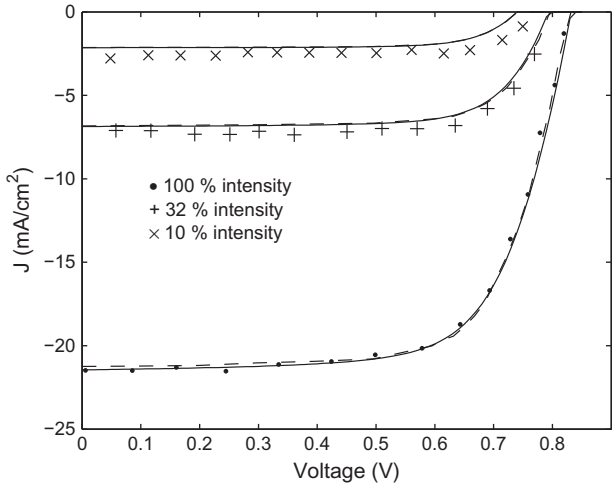

Fig. 3. Net current density versus voltage at three sun intensities. The symbols represent experimental data and the solid lines represent the theoretical fit to the experimental data. The experimental data were extracted from Ref. [5].

an average drift velocity of the carriers throughout the absorber layer will not make any significant difference in the calculation of charge collection. The theoretical results in the rest of this paper are based on the analytical model.

The best fit $\mu\tau'$ of holes and electrons are $\mu_h\tau'_h = 4\times 10^{-6}$ cm^2/V and $\mu_e\tau'_e = 1.8\times 10^{-5}$ cm^2/V, which are consistent with the $\mu\tau'$ values in CdTe [12]. Assuming typical values for CdTe layer, μ_h = 20 cm^2/V s and μ_e = 180 cm^2/V s [5], the carrier lifetimes become, $\tau'_h = 0.2$ μs and $\tau'_e = 0.1$ μs. Note that a similar fitting was obtained by the previous model [5] using three additional fitting parameters (maximum photocurrent with complete charge collection, reverse saturation current, an effective attenuation coefficient for the whole solar spectrum). Moreover, it also failed to distinguish the electron and hole transport properties and thus mentioned an effective mobility-lifetime product of 9×10^{-7} cm^2/V by fitting the experimental data with the single carrier Hecht collection efficiency formula. The other fitted parameters in Fig. 2 are: V_0 = 0.85 V, A = 1.95, R_s = 3.5 Ω cm^2, and R = 0.175. The diode quality factor is 1.9, which implies that the recombination current dominates over the diffusion current.

The EHPs are generated exponentially across the CdTe layer. Since the photon absorption coefficient up to 900 nm of wavelength is very high, the EHPs are mainly generated near the *n-p* interface in the CdTe layer. Therefore, electrons quickly move towards the top electrode and holes have to move a much longer distance towards the bottom electrode. Thus, the charge collection should mainly be controlled by the hole transport properties [13]. Fig. 4a and b shows the *J–V* characteristics of CdS/CdTe solar cells for various levels of $\mu\tau'$ products of holes and electrons. All other parameters in Fig. 4 are the same as in Fig. 3. The theoretical overall efficiency varies from 8.2% to 14.3% by changing the $\mu_h\tau'_h$ values from 5×10^{-7} cm^2/V to 10^{-4} cm^2/V, whereas it varies from 10.3% to 12.4% by changing the $\mu_e\tau'_e$ values from 10^{-7} cm^2/V to 10^{-4} cm^2/V. As evident from Fig. 4a and b that the *J–V* characteristics is much more sensitive to the hole transport than to the electron transport. The efficiency is reduced drastically if $\mu_h\tau'_h$ is less than 10^{-6} cm^2/V. It increases slightly with increasing $\mu_h\tau'_h$ above 10^{-5} cm^2/V.

The performance of CdTe solar cells may degrade over time and the extent of the degradation depends on the absorber and contact materials. Fig. 5 shows the *J–V* characteristics of a CdTe solar cell with a bilayer back contact of 15 nm Cu/50 nm Ni before and after stress. The CdTe layer thickness is 7 μm. The stressing was done by

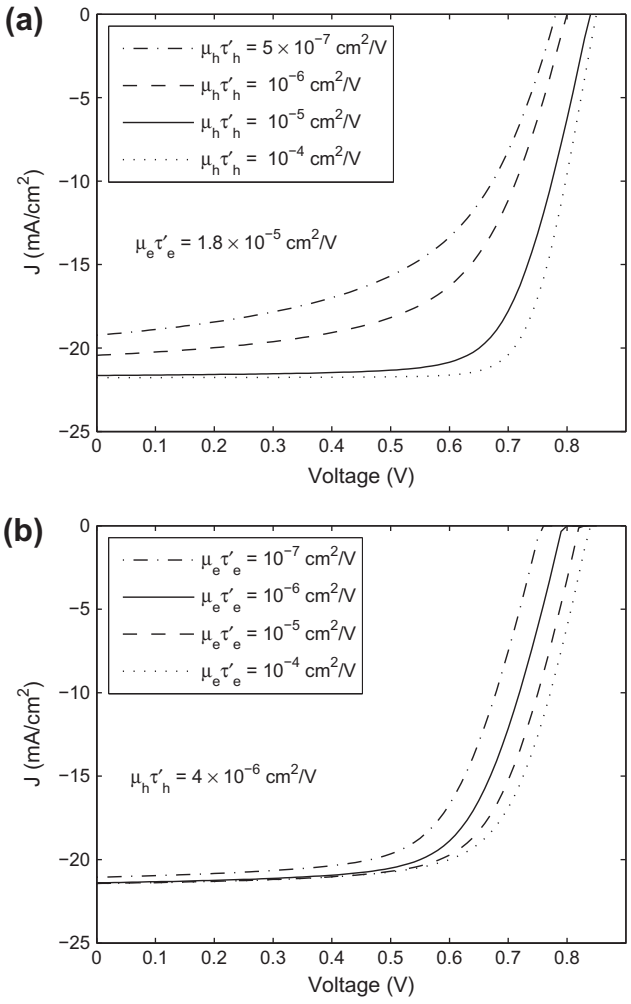

Fig. 4. Theoretical net current density versus voltage for various levels of $\mu\tau'$ products of holes and electrons in CdTe solar cells.

keeping the cell at 85 °C in dry air at 100% sun illumination at open circuit for 15 days. Assuming typical values for CdTe layer, μ_h = 20 cm^2/V s and μ_e = 180 cm^2/V s, the best fit parameters before stress are $\tau'_h = 0.8$ μs, $\tau'_e = 1$ μs, V_0 = 0.81 V, A = 1.9, R_s = 3.5 Ω cm^2, and R = 0.1, whereas after stress the fitted parameters are $\tau'_h = 0.38$ μs, $\tau'_e = 0.6$ μs, V_0 = 0.77 V, A = 1.9, R_s = 5.2 Ω cm^2, and R = 0.1. The overall efficiency varies from 13.4% to 10.6% due to this long time stress. The carrier lifetimes and series resistance deteriorate because of long term stress, which indicates that the transport properties of the CdTe and CdS layers degrade slightly due to stress in cells with the Cu back contact.

3.2. CIGS solar cells

The model is applied to GIGS solar cells. The absorption coefficient for CIGS is obtained from the absorption curves in Ref. [14]. Fig. 6 shows the *J–V* curves of a GIGS solar cell at 100% sun intensity. The symbols represent experimental data and the solid lines represent the theoretical fit to the experimental data. The experimental data were extracted from Fig. 7 of Ref. [3]. The dotted line represents complete charge collection and no series loss, the dashed line represents incomplete charge collection in the absorber layer and no series loss, and the solid line represents the theoretical fit based on the present model. The CIGS thickness is 2 μm. The CdS thickness is assumed as 0.1 μm. The theoretical model shows a very

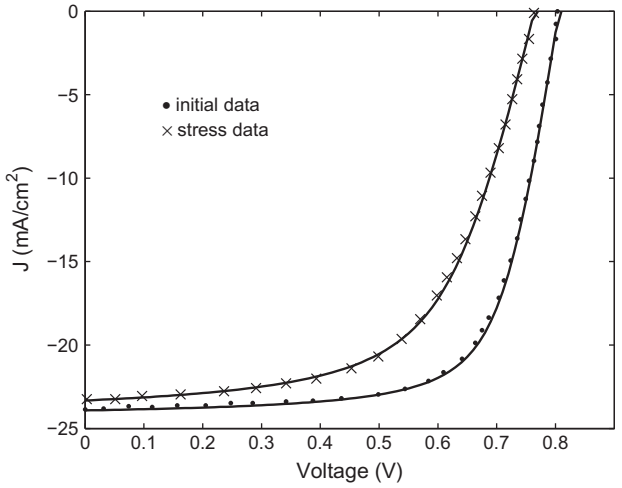

Fig. 5. Current–voltage characteristics of a CdTe solar cell before and after stress. The symbols represent experimental data and the solid lines represent the theoretical fit (analytical model) to the experimental data. The experimental data were extracted from Ref. [5].

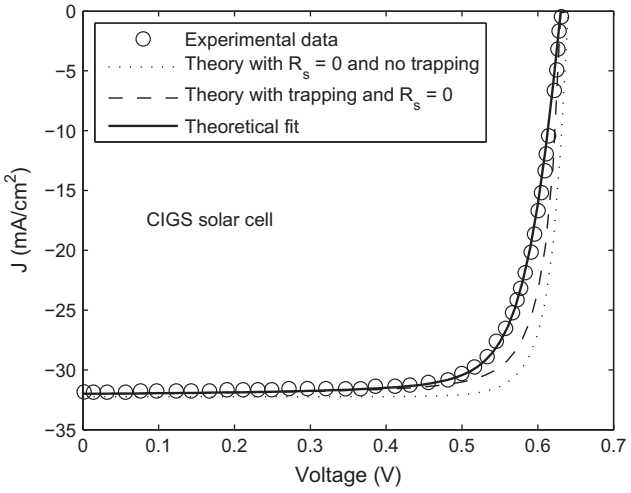

Fig. 6. Current–voltage characteristics of a CIGS solar cell. The symbols represent experimental data that were extracted from Ref. [3]. The dotted line: complete charge collection and no series loss, the dashed line: incomplete charge collection in the absorber layer and no series loss, and the solid line: the theoretical fit based on the analytical model.

good agreement with the experimental data. The best fit parameters are $\mu_h\tau'_h = 4\times10^{-6}$ cm^2/V and $\mu_e\tau'_e = 5\times10^{-6}$ cm^2/V, $V_0 = 0.64$ V, $A = 1.53$, $R_s = 0.5\ \Omega$ cm^2, and $R = 0.23$. The overall efficiency is 15.5%. The short circuit current density is 31.8 mA/cm^2 and the shape of the *J–V* curve is almost rectangular, which indicates that the carrier transport properties in CIGS are very good. The difference between the dotted line and the solid line represents the effects of the carrier transport properties on the *J–V* characteristics, which is small in CIGS solar cells. The CIGS material can efficiently absorb the incident photons up to 1200 nm of wavelength, which gives high short circuit current and high overall efficiency.

3.3. Amorphous Si solar cells

The model can also be applied to a-Si:H *p-i-n* solar cells. The absorption coefficient for amorphous silicon is obtained from the absorption curves in Ref. [15]. Fig. 7 shows the *J–V* curves of a GIGS solar cell at 100% sun intensity. The symbols represent

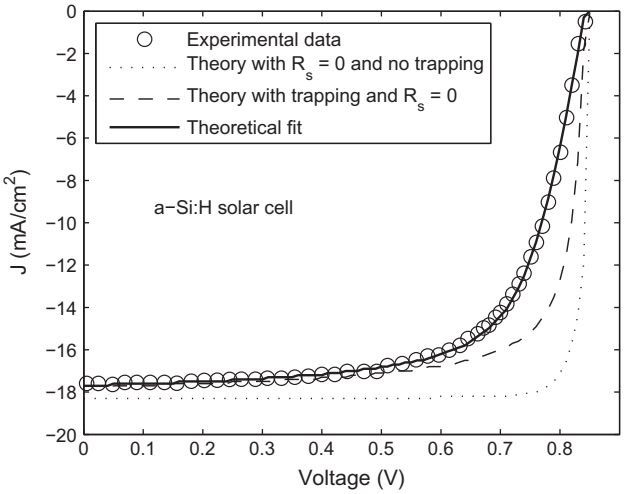

Fig. 7. Current–voltage characteristics of an a-Si:H solar cell. The symbols represent experimental data that were extracted from Ref. [16]. The dotted line: complete charge collection and no series loss, the dashed line: incomplete charge collection in the absorber layer and no series loss, and the solid line: the theoretical fit based on the analytical model.

experimental data and the solid lines represent the theoretical fit to the experimental data. The experimental data were extracted from Fig. 1 of Ref. [16]. The *i*-layer thickness is 2 μm. The theoretical model shows a very good agreement with the experimental data. The best fit $\mu\tau'$ of holes and electrons are $\mu_h\tau'_h = 0.6\times10^{-8}$ cm^2/V and $\mu_e\tau'_e = 1.5\times10^{-6}$ cm^2/V, which are consistent with the $\mu\tau'$ values in a-Si:H [17,18]. The other fitted parameters in Fig. 7 are $V_0 = 0.85$ V, $A = 1.6$, $R_s = 4\ \Omega$ cm^2, and $R = 0.1$. The a-Si:H material can efficiently absorbs the incident photons up to 820 nm of wavelength. The overall efficiency is 10.2% and the short circuit current is 17.6 mA/cm^2. It is evident from Fig. 7 that the *J–V* characteristics significantly depend on the carrier transport properties in *i*-layer.

4. Conclusions

An analytical model to study the current–voltage characteristics of thin film solar cells has been developed. An analytical expression for the external voltage dependent photocurrent is derived by considering exponential electron–hole pair generation, carrier trapping and carrier drift in the absorber layer. The overall load current is calculated considering the forward dark current and the actual solar spectrum. The recombination current in the depletion region dominates over the ideal diode current in CdTe solar cells. The solar cell efficiency depends critically on the transport properties of the carriers that drift towards the back contact. The photon absorption capability over a wide spectrum and good carrier transport properties of the absorber layer are equally important for achieving higher efficiency. The analytical model shows a very good agreement with the published experimental data on various thin film solar cells.

Acknowledgment

The authors acknowledge financial supports from NSERC.

References

[1] Green MA, Emery K, Hishikawa Y, Warta W. Prog Photovolt Res Appl 2010;18:144–50.
[2] Nelson J. The physics of solar cells. Imperial College Press; 2003 [chapter 8].
[3] Hegedus SS, Shafarman WN. Prog Photovolt Res Appl 2004;12:155–76.
[4] Hegedus SS. Prog Photovolt Res Appl 1997;5:151–68.

[5] Hegedus S, Desai D, Thompson C. Prog Photovolt Res Appl 2007;15:587–602. and references therein.
[6] Sah C-T, Noyce RN, Shockley W. Proc Inst Radio Eng 1957;45:1228.
[7] Mishra UK, Singh J. Semiconductor device physics and design. Netherlands: Springer; 2008 [chapter 4].
[8] Shockley W. J Appl Phys 1938;9:635–6.
[9] Iverson AE, Smith DL. IEEE Trans Electron Dev 1987;ED-34:2098–107.
[10] NREL; November 2010 <http://rredc.nrel.gov/solar/spectra/am1.5/>.
[11] Burgelman M. In: Poortmans J, Arkhipov V, editors. Thin film solar cells: fabrication, characterization and applications. England: Wiley & Sons; 2006 [chapter 7].
[12] Metzger WK, Albin D, Levi D, Sheldon P, Li X, Keyes BM, et al. J Appl Phys 2003;94:3549.
[13] Kabir MZ, Kasap SO. Appl Phys Lett 2002;80:1664.
[14] Hana S-H, Hermann AM. Appl Phys Lett 2004;85:576–8.
[15] Sze SM. Semiconductor devices: physics and technology, 2nd ed. USA: John Wiley & Sons; 2002 [chapter 9].
[16] Klimovsky E, Rath JK, Schropp REI, Rubinelli FA. J Non-Cryst Solids 2004;338–40:686–9.
[17] Street RA, editor. Technology and applications of amorphous silicon. Springer-Verlag; 2000. p. 151.
[18] Jackson WB, Kelso SM, Tsai CC, Allen JW, Oh S-J. Phys Rev B 1985;31:5187.